Superlattices and Microstructures 103 (2017) 245–251

Contents lists available at ScienceDirect

Superlattices and Microstructures

journal homepage: www.elsevier.com/locate/superlattices

Internal quantum efficiency and Auger recombination in green, yellow and red InGaN-based light emitters grown along the polar direction

Thi Huong Ngo [a, *], Bernard Gil [a], Benjamin Damilano [b], Kaddour Lekhal [b], Philippe De Mierry [b]

[a] Laboratoire Charles Coulomb-UMR 5221-CNRS, Université Montpellier, Case Courrier 074, 34095, Montpellier, Cedex 5, France
[b] CRHEA-CNRS-Centre de Recherches sur l'Hétéro-Epitaxie et ses Applications, Centre National de la Recherche Scientifique, 06560, Valbonne, France

ARTICLE INFO

Article history:
Received 14 January 2017
Accepted 16 January 2017
Available online 20 January 2017

ABSTRACT

We comparatively study the onset of photo-induced non-radiative intrinsic Auger recombination processes for red, yellow and green light emitting InGaN–GaN heterostructures grown along the polar orientation. We find a dramatic reduction of the photo excitation densities triggering the domination of Auger effect with increasing emission wavelength; that is to say in concert with the enhancement of the internal electric field in the structure. In long wavelength emitters, the internal electric field is stronger, and hence reducing the impact of the internal electric field is more critical.

1. Introduction

The realization of nitride-based optoelectronic devices with high internal quantum efficiency (IQE) and that operate in the region of the light spectrum scaling from the green to the red has been tantalizing researchers since the birth of the blue light emitting diode [1]. In this report, we investigate one of the factors that limit the potentialities of III-nitrides, for the realization of optoelectronic devices susceptible to operate efficiently in that critical range of wavelengths: the quantum confined Stark effect (QCSE). We study comparatively the light-matter interaction process in structures based on InGaN multiple quantum wells (MQWs), emitting green, yellow and red light submitted to a large range of photo excitation densities. These colours of light emitter are obtained by tuning both the QCSE and the carrier localization in indium-rich regions of the QW layers. In some cases, AlGaN layers have been intercalated in the heart of the heterostructures in order to alter the electric field (by increasing the chemical contrast at hetero interfaces), and to compensate the built-in strain to prevent as much as possible the generation of dislocations. This reduces the value of the non-radiative recombination rate. The IQE dramatically decreases under high photo injection densities in correlation with efficient nnp intrinsic Auger nonradiative recombinations [2]. We find that, the stronger QCSE, that is to say the impact of the electric field on the radiative recombination rate, the lower the onset of dominant Auger related intrinsic non-radiative recombination, as expected from the recent review papers of Refs. [3,4].

Contributions of the radiative and non-radiative recombination rates were fitted using the phenomenological ABC model which, without pretending to any quantitative microscopic description of their mechanisms, gives a global overview of the

* Corresponding author.
E-mail address: thi-huong.ngo@umontpellier.fr (T.H. Ngo).

http://dx.doi.org/10.1016/j.spmi.2017.01.026
0749-6036/

different phenomena that are competing [5,6]. We find that adding an AlGaN strain compensating layer reduces the Shockley-Read Hall non-radiative recombination (A parameter) more efficiently for the red-light emitting sample compared to the yellow-light emitting one. We also find that the collapse of the IQE occurs at photo-excitation densities that decrease with the increase of the indium content in the QW. The most efficient localization of the carriers in indium-rich regions of the QW seems to favour intrinsic non-radiative Auger recombination relatively to the intrinsic radiative one [7,8]. Therefore, both QCSE and carrier localization in energetically favourable parts of the QW contribute in concert to the efficiency of the Auger effect.

2. Experimental

Designs of green-light (sample G) and yellow-light (sample Y) samples were previously reported by Lekhal et al. (as sample A and sample A2 in Ref. [9]). In order to keep identical indium composition (0.21) and QW thickness (2.6 nm) for the InGaN QW of the two samples, the growth conditions of the well layers are kept identical. The barrier layer of sample G was grown without AlGaN layer while the barrier of sample Y was grown including a 5.2 nm-thick AlGaN layer. Then, a red-light emitting sample (sample R) is grown under the same conditions as sample Y, except that the growth temperature of InGaN QW is decreased from 715 °C to 700 °C. Consequently, the indium composition is larger in sample R than in sample Y and sample G. The comparison between the growth parameters of the different samples can be found in Table 1.

Time-resolved photoluminescence (TRPL) spectroscopy and photoexcited power-dependence (PPD) spectroscopy experimental measurements were carried out in term of in experimental conditions identical to those reported in Ref. [2]. The samples are cooled to 8 K by using a cryostat with helium flow in both kinds of measurements. In the TRPL measurement, we use the second harmonic/third harmonic (wavelength at 400nm/266 nm) of a Ti:sapphire laser with pulse repetition rate at 80 kHz as excitation source. Power density is kept at 0.4 Wcm^{-2} as a low excitation condition. For the PPD measurement, a third harmonic is used to excite the samples with the repetition rate of the laser is selected at 80 MHz. Under these conditions, the PPD measurement is considered as continuous wave (CW) photoluminescence (PL) spectroscopy measurement. The power density of laser for this measurement is varied through 5 decades from 1.2×10^{-2} Wcm^{-2} to 3.7×10^{3} Wcm^{-2}.

3. Results

Fig. 1(a)-(c) report a series of low temperature CW PL spectra recorded for sample R, sample Y and sample G. In the inset are plotted highly magnified PL spectra recorded in the low excitation range. The side peaks at higher energy (2.75 eV in the green sample, 2.45 eV in the yellow and in the red samples) are generated by thickness/composition inhomogeneity in InGaN–GaN heterostructures [11]. The second additional peak of the red sample at 2.25 eV is origin from the yellow band of the GaN barrier layer [12,13]. Plotting the logarithm of the PL intensities against the logarithm of the excitation power densities gives unity slopes up to photo excitation densities noted P_T as shown in Fig. 2(a). Then sublinear dependences are recorded. P_T equals 4 Wcm^{-2} for sample R. Beyond this value the slope passes from 1 to 0.85. This sublinear dependence is the evidence of Auger-type non-radiative recombination [14,15]. The photo excitation densities at the threshold for the linear to sublinear dependences are 40 Wcm^{-2}, and 500 Wcm^{-2} for samples Y and G respectively as shown in Table 1, and the slopes beyond these values are 0.84 and 0.87 respectively. The important experimental result that we emphasize here is the onset of sublinear dependence with pump power which decreases when increasing the emission wavelength.

We remark that there is an energy blue-shift of the PL feature which starts at 1 Wcm^{-2} for sample R and reaches in this case about 90 meV without saturating in the range of our experimental densities of photo excitation. This blue-shift is due to the screening of the internal electric field by photo-injected carriers and also to phase-space filling effect. We have plotted the evolution of such blue-shift for samples R, Y and G against photo-excitation density in Fig. 2(b). The energy shifts indicate that the drops of the potential line-ups are decreasing from sample R to sample Y, to sample G, as expected from the physics of nitride hetero-structures grown along the polar orientation. This is the first indication of the increasing impact of QCSE in the QW structure with the increase of emission wavelength [16].

To frame the relative contribution of radiative and non-radiative recombination rates, we begin by the determination of the IQE. The IQE at low excitation level was first deduced from low temperature time-resolved (TR) PL experiments according to the method initiated by Iwata et al. [17] for kinetics of PL ruled by two-exponential decays. This is very convenient for the determination of IQE in the case of yellow light emitters [18] and more general in reasonably inhomogeneous samples [17].

Table 1
Characteristic parameters of the samples: t_{G_InGaN}, and T_{G_InGaN} are the growth time and the growth temperature of InGaN quantum well, respectively. L_{InGaN}, L_{AlGaN}, L_{GaN}, and In are the thickness of (In,Ga)N, $Al_{0.2}Ga_{0.8}N$, GaN barrier layers and the indium composition, respectively. WL, P_T, F are the peak wavelength of emitter, the threshold of excitation density for the transition from linear to sublinear of evolution of integrated PL intensity versus excitation power density, and the internal electric field in the InGaN quantum well, respectively.

Sample	t_{G_InGaN} (s)	T_{G_InGaN} (° C)	L_{InGaN} (nm)	In (%)	L_{AlGaN} (nm)	L_{GaN} (nm)	WL (nm)	P_T (W/cm^{-2})	F ($MVcm^{-1}$)
R	120	700	2.6	23	5.2	11.9	615	4	3.7
Y	120	715	2.6	21	5.2	11.9	565	40	3.5
G	120	715	2.6	21	0	15.2	515	500	2.9

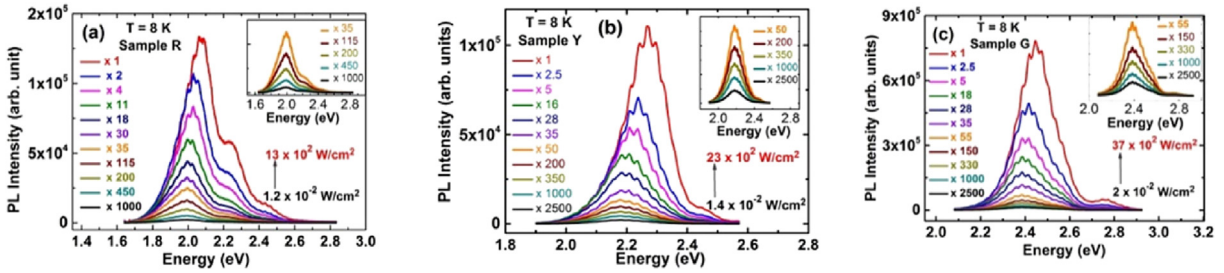

Fig. 1. (a) Evolution of the photoluminescence spectra at 8 K versus power excitation for sample R. The photoluminescence spectra are multiplied by factors: ×1000, ×450, etc. when excitation power density increases from 1.2×10^{-2} to 3.7×10^{3} W/cm^2. Inset: photoluminescence spectra in the low photo-excitation densities range. (b) and (c) are the analogous of (a) for samples Y and G, respectively.

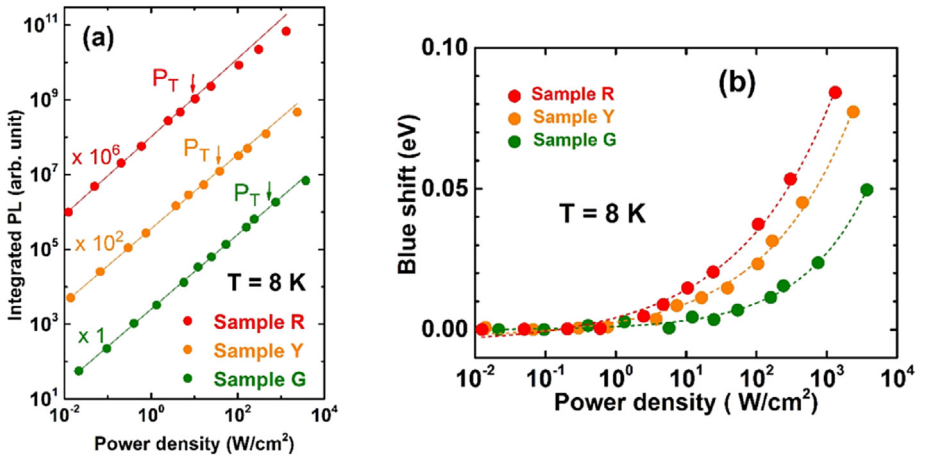

Fig. 2. (a) Logarithm plotting of the integrated photoluminescence intensities (circles) against the excitation power density. The lines correspond to a linear fit of the data in the excitation power density range. The arrows show the position of P_T. (b) The blue shift of all samples plotted as a function of logarithmic of the excitation density. The blue shift decreases from sample R to sample Y, and to sample G. (For interpretation of the references to colour in this figure legend, the reader is referred to the web version of this article.)

The low temperature PL transients, the values of the slow decay times (radiative component) and the values of the IQE for all samples listed in Table 2. We find that, the values of IQE at low excitation level increase with the emission wavelength. This evidences the reduction of non-radiative recombination processes in longer wavelength-emitting samples, in correlation with the decreasing of defect density achieved by the intercalation of the AlGaN strain compensating layer. The fast decay time τ_{fast} of sample R is fitted larger than for samples Y and G, indicating that the non-radiative recombination rate in sample R is lower than that in samples Y and G. This leads to an enhancement of the IQE for sample R. We attribute this result to the large indium composition which, from simple binomial statistical arguments, leads to increased fluctuations of chemical compositions in sample R [7,8,19–21], and therefore, enhances the localization of carriers at indium-rich which prevents their migration towards non-radiative recombination centers.

Besides the increase of the IQE with emission wavelength, an increase of the radiative decay time was measured from sample G to sample R. This is the second experimental indication of an increase of the value of the internal electric field in the InGaN layers from sample G to sample R. The values of the internal electric field are determined by using the same calculation reported in Ref. [9]. These values are listed in Table 1. An importance consequence of the increase of the internal electric field is the reduction of the threshold corresponding to dominant Auger recombination.

To go further details of the comprehension of the experimental results observed here, we have computed the evolution of the IQE with photo-excitation densities from the integrated PL intensity I_{PL}, and the generation rate G [22].

$$IQE = \frac{I_{PL}}{\eta G}, \tag{1}$$

The constant value of η is determined by using values of I_{PL}, G, and IQE at low excitation level.
The values of the generation rate G were calculated directly from the experimental conditions

Table 2
Low temperature characteristics decay times τ_{fast}, τ_{slow}, IQE_{LT} and IQE_{RT} are the IQE at low temperature and room temperature, respectively.

Sample	Peak WL (nm)	τ_{fast} (ns)	τ_{slow} (ns)	IQE_{LT} (%)	IQE_{RT} (%)
R	615	165.2	562.5	56	1.7
Y	565	49.6	199.9	54	2.6
G	515	8.5	29.6	50	2.4

$$G = \frac{P_{laser}(1-R)\alpha}{A_{spot}(h\upsilon)} \tag{2}$$

where P_{laser} is the incident laser power, R is the reflection coefficient at the semiconductor-to-air interface, α is the absorption coefficient of the light in the semiconductor which may vary with the carrier density, that is to say with the screening of QCSE, $h\upsilon$ is the incident photon energy, A_{spot} is the surface of the laser spot.

The carrier density is extracted from experimental value of the IQE, the generation rate and the measured value of the radiative decay time by equation:

$$n = IQE \times G \times \tau_r, \tag{3}$$

The evolution of the IQE versus pump power is plotted using spheres in Fig. 3. It clearly shows that the onset of efficiency droop occurs at lower excitation densities in case of sample R than in cases of sample Y and sample G. The higher internal electric field, the more dramatic impact of QCSE for increasing the carrier decay times. Therefore, at a given photo-carrier density, the density of photo-generated carriers is higher in the red emitting sample than others, as reported hereafter, thanks to the dominating influence of the variation of τ_r of equation (3). The number of collisions which increases with the third power of the carrier density ($\sim n^3$) favours the promotion of excess electronic energy and eventual electronic escape away from the active region [23,24].

We estimate the contribution of Shockley-Read-Hall non-radiative recombination, radiative recombination, and Auger non-radiative recombination by fitting the experimental IQE using a modified ABC model that includes the residual n-type doping [25]. Value of the residual doping is estimated about 4.8×10^{18} cm^{-3} for all samples. In this model, under steady-state conditions, the generation rate can be determined by expression:

$$G = \frac{n(n+n_0)}{\tau_n n + \tau_p(n+n_0)} + Bn(n+n_0) + C_n n(n+n_0)^2 + C_p n^2(n+n_0), \tag{4}$$

where n is the excess of photo-created electron (or hole) density, n_0 is the residual doping, τ_n and τ_p are the minority carrier lifetimes for the n-type and p-type semiconductor, respectively, B, C_n and C_p are coefficient of radiative recombination, nnp-Auger, and npp-Auger recombination, respectively.

In the absence of residual doping, the coefficient of Shockley-Read-Hall nonradiative recombination is defined as $A = (\tau_n + \tau_p)^{-1}$. By approximating that $\tau_n = \tau_p$, we have $\tau_n = \tau_p = 1/2$ A.

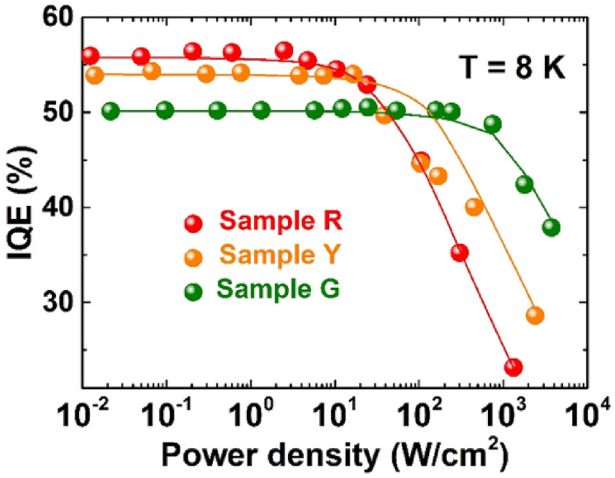

Fig. 3. Experimental internal quantum efficiency (spheres) of all samples plotted as a function of the excitation power density. Fitting curves are showed as solid lines.

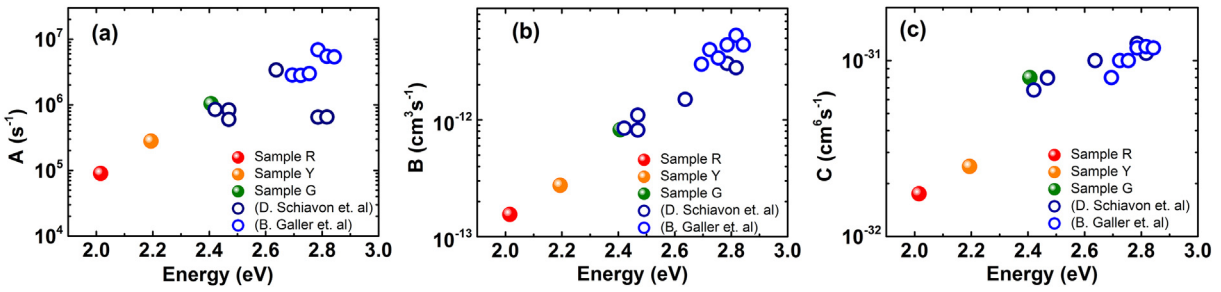

Fig. 4. (a)–(c) Evolution of coefficients A, B and C (in logarithmic scale) versus emission energy. The spheres show our fitted data for sample R, Y and G. The circles display the data reported by D. Schiavon et al. [26] and B. Galler et al. [27], respectively.

Galler et al. demonstrated in Ref. [25] that the efficiency droop is dominated by nnp-type Auger recombination rather than npp-type for an n-type InGaN material. Therefore, we assume here that $C_p = 0$ for our n-doped samples.

Then, the generation rate in Eq. (4) can be rewritten by a simpler expression

$$G = \frac{2An(n + n_0)}{2n + n_0} + Bn(n + n_0) + C_n n(n + n_0)^2 \tag{5}$$

The theoretical IQE is calculated by equation

$$IQE = \frac{Bn(n + n_0)}{G}, \tag{6}$$

The fitted curves (theoretical IQE) are displayed in Fig. 3 as solid lines and the fitting parameters are summarized in Fig. 4. We find a decreasing trend for all the coefficients A, B, and C with increasing emission wavelength. A similar trend is obtained in InGaN single QWs by D. Schiavon et al. [26], and B. Galler et al. [27]. Obviously, the behaviours we evidence and quantify here extrapolate the trends previously reported in other samples.

4. Discussion

In the following, we discuss the relative variations of the A, B, C coefficients in our different samples. The recent works dedicated to the reduction of the defect density related to the built-in strain field in case of long wavelength region of the visible light emitting hetero-structures based on MQWs InGaN–GaN with AlGaN strain compensating layers [9,28–30]. By correctly designing the thickness of the different layers, lattice-matching of a GaN–InGaN–AlGaN three-material structure to GaN can be obtained as indicated by the X-ray diffraction measurements reported in Ref. [9]. We previously clearly correlated the enhancement of the room temperature and low temperature PL intensities with the reduction of defect densities by adding an AlGaN strain-compensating layer [18]. This contributes here to the decrease of the value of A from samples Y to R. We have also to remind that the indium composition increases from sample G to sample R, which leads to deeper localization potentials [20,21] and prevents the escape of the carriers out of the active parts of the MQWs. The both contributions decrease the values of A from sample G to sample R: $A_{Green} > A_{yellow} > A_{red}$.

The increase of the internal electric field reduces the electron and hole wave functions overlap from sample G to sample R and subsequently increase the radiative decay time τ_r. This leads to $B_{Green} > B_{yellow} > B_{red}$. David and Grundmann [31,32] have studied the evolution of B with electron densities and they have shown that, in case of blue light emitters, it decreases at high densities (larger than10^{18} cm^{-3}). We have decided to reduce here value of B with carrier density by a form $B(n) = B_0/[1+(n/n_{psf})^{\gamma}]$, as plotted in Fig. 6 (c) where B_0 is value of coefficient B at low excitation density [33] (plotted as spheres in Fig. 4(b)), $n_{psf} = 2 \times 10^{19}$ cm^{-3} is the carrier density for the onset of phase-space filling effect, $\gamma = 0.82$ is a dimensionless exponent [34]. Moreover, under high excitation condition, the Coulomb interaction of carrier increase that cause a reduction in decay time of samples, as shown in Fig. 6(a) [31,35].

Regarding to the values of C, there is a correlation with the values of B as sketched in Fig. 5 where we have also reported the data collected by Weisbuch et al. [3,32,36,37] and the data of Schiavon et al. [26], and Galler et al. [27]. This indicates that the values of C can be framed with an approximation using a scaling argument and from the values of B obtained by TRPL spectroscopy. The localization phenomena have a dominating impact at the scale of the radiative decay time that is to say at the scale of the radiative recombination rate. We can thus reasonably anticipate from our experimental results of their determinant impact at the scale of the intrinsic non-radiative Auger recombination. It is proportional to cubic of carrier density (n^3) in the samples. Fig. 6(b) shows that the carrier density in the red sample is approximate 10 times or 3 times larger than in the green or in the yellow samples. Therefore, non-radiative Auger recombination in the red sample is much stronger than in the two other samples even values of the coefficient C is smaller in the red sample.

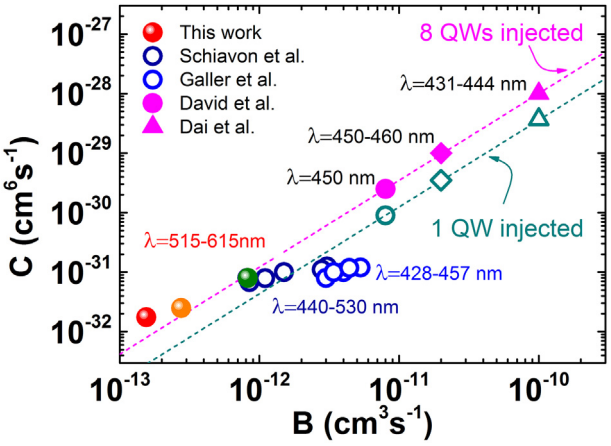

Fig. 5. Evolution of coefficient C as a function of coefficient B for our own data (MQWs, spheres) compared with the compilation by Weisbuch et al. [3,32,36,37] and the complementary data of Schiavon et al. [26], and Galler et al. [27] for single QWs.

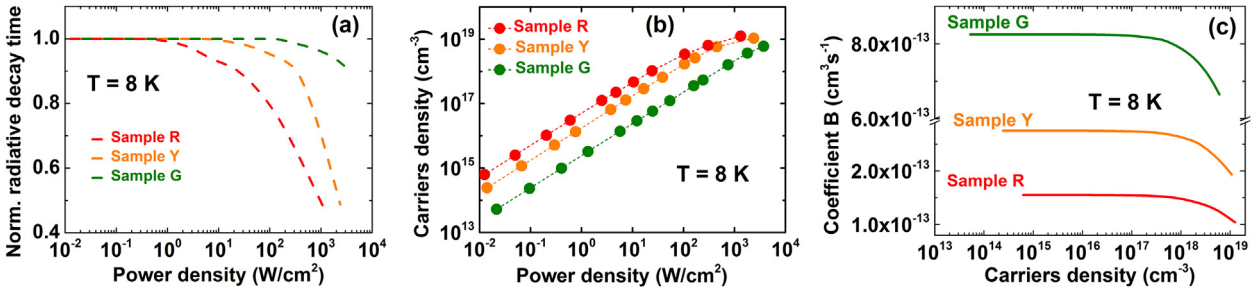

Fig. 6. (a) Evolution decay time of all samples with the power density. (b) Carrier density as a function of the power density; Dotted lines are the eyes guidance. (c) Evolution of the coefficient B as a function of the carrier density.

In conclusion, by comparatively studying recombination processes for polar orientated red, yellow, and green InGaN-(Al)GaN QWs, we find that the onset of efficiency droop occurs at lower photo excitation densities when the QW emission wavelength increases. This is correlated to the enhancement of the internal electric field in the active part. QCSE plays in concert with the localization of carriers in energetically favourable regions of the QWs.

Acknowledgments

We acknowledge the extensive support, including the PhD grant to Thi Huong Ngo, from GANEX (ANR-11-LABX-0014). GANEX belongs to the publicly funded “Investissements d'Avenir” program managed by the French ANR Agency.

References

[1] S. Nakamura, M.R. Krames, History of gallium–nitride-based light-emitting diodes for illumination, Proc. IEEE 101 (10) (October 2013) 2211–2220.
[2] T.H. Ngo, B. Gil, P. Valvin, B. Damilano, K. Lekhal, P. De Mierry, Internal quantum efficiency in yellow-amber light emitting AlGaN-InGaN-GaN heterostructures, Jpn. J. Appl. Phys. 55 (2016) 05FG10.
[3] C. Weisbuch, et al., The efficiency challenge of nitride light-emitting diodes for lighting, Phys. Status Solidi A 212 (2015) 899–913.
[4] B. Damilano, B. Gil, Yellow–red emission from (Ga,In)N heterostructures, J. Phys. D. Appl. Phys. 48 (2015) 403001.
[5] M. Binder, et al., Identification of nnp and npp Auger recombination as significant contributor to the efficiency droop in (GaIn)N quantum wells by visualization of hot carriers in photoluminescence, Appl. Phys. Lett. 103 (2013) 071108.
[6] M. Amani, et al., Near-unity photoluminescence quantum yield in MoS_2, Science 350 (2015) 1065.
[7] D. Watson-Parris, et al., Carrier localization mechanisms in InxGa1−xN/GaN quantum wells, Phys. Rev. B 83 (2011) 115321.
[8] P. Dawson, S. Schulz, R.A. Oliver, M.J. Kappers, C.J. Humphreys, The nature of carrier localisation in polar and nonpolar InGaN/GaN quantum wells, J. Appl. Phys. 119 (2016) 181505.
[9] K. Lekhal, et al., Strain-compensated (Ga,In)N/(Al,Ga)N/GaN multiple quantum wells for improved yellow/amber light emission, Appl. Phys. Lett. 106 (2015) 142101.
[11] Z. Li, et al., Two distinct carrier localization in green light-emitting diodes with InGaN/GaN multiple quantum wells, Appl. Phys. Lett. 115 (2014) 083112.
[12] P. Hacke, et al., Characterization of the Shallow and Deep levels in Si-doped GaN grown by metal-organic vapor phase epitaxy, Jpn. J. Appl. Phys. 33 (1994) 6443.
[13] W. Grieshaber, et al., Competition between band gap and yellow luminescence in GaN and its relevance for optoelectronic devices, J. Appl. Phys. 80 (1996) 4615.

[14] K.D. Glinchuk, A.V. Prokhorovich, V.I. Vovnenko, Study of non-linear extrinsic luminescence in GaAs, Phys. Status Solidi A 54 (1979) 121.
[15] E. O'Hara, J.R. Gullingsrud, J.P. Wolfe, Auger decay of excitons in Cu2O, Phys. Rev. B 60 (1999) 10872.
[16] B. Gil, Physics of Wurtzite Nitrides and Oxides, Springer, Berlin, 2014, p. 192.
[17] Y. Iwata, R.G. Banal, S. Ichikawa, M. Funato, Y. Kawakami, Emission mechanisms in Al-rich AlGaN/AlN quantum wells assessed by excitation power dependent photoluminescence spectroscopy, J. Appl. Phys. 117 (075701) (2015).
[18] T.H. Ngo, B. Gil, P. Valvin, B. Damilano, K. Lekhal, P. De Mierry, Internal quantum efficiency in yellow-amber light emitting AlGaN-InGaN-GaN heterostructures, Appl. Phys. Lett. 107 (2015) 122103.
[19] B. Gil, Physics of Wurtzite Nitrides and Oxides, Springer, Berlin, 2014, pp. 171–174.
[20] M. Filoche, S. Mayboroda, Universal mechanism for Anderson and weak localization, PNAS 109 (37) (2012) 14761–14766.
[21] T.-J. Yang, R. Shivaraman, J.S. Speck, Y.-R. Wu, The influence of random indium alloy fluctuations in indium gallium nitride quantum wells on the device behavior, J. Appl. Phys. 116 (2014) 113104.
[22] Dai, et al., Internal quantum efficiency and nonradiative recombination coefficient of GaInN/GaN multiple quantum wells with different dislocation densities, Appl. Phys. Lett. 94 (2009) 111109.
[23] J. Iveland, L. Martinelli, J. Peretti, J.S. Speck, C. Weisbuch, Direct measurement of auger electrons emitted from a semiconductor light-emitting diode under electrical injection: identification of the dominant mechanism for efficiency droop, Phys. Rev. Lett. 110 (2013) 177406.
[24] J. Peretti, et al., Identification of Auger effect as the dominant mechanism for efficiency droop of LEDs, Proc. SPIE. 9003 (2014) 90030Z.
[25] B. Galler, et al., Experimental determination of the dominant type of auger recombination in InGaN quantum wells, Appl. Phys. Express 6 (2013) 112101.
[26] D. Schiavon, et al., Wavelength-dependent determination of the recombination rate coefficients in single-quantum-well GaInN/GaN light emitting diodes, Phys. Status Solidi B 250 (2013) 283.
[27] B. Galler, et al., Influence of indium content and temperature on Auger-like recombination in InGaN quantum wells grown on (111) silicon substrates, Appl. Phys. Lett. 101 (2012) 131111.
[28] T. Shioda, H. Yoshida, K. Tachibana, N. Sugiyama, S. Nunoue, Enhanced light output power of green LEDs employing AlGaN interlayer in InGaN/GaN MQW structure on sapphire (0001) substrate, Phys. Status Solidi A 209 (2012) 473.
[29] S. Saito, R. Hashimoto, J. Hwang, S. Nunoue, InGaN light-emitting diodes on c-face sapphire substrates in green gap spectral range, Appl. Phys. Express 6 (2013) 111004.
[30] J.I. Hwang, R. Hashimoto, S. Saito, S. Nunoue, Development of InGaN-based red LED grown on (0001) polar surface, Appl. Phys. Express 7 (2014) 071003.
[31] A. David, M.J. Grundmann, Droop in InGaN light-emitting diodes: a differential carrier lifetime analysis, Appl. Phys. Lett. 96 (2010) 103504.
[32] A. David, M.J. Grundmann, Influence of polarization fields on carrier lifetime and recombination rates in InGaN-based light-emitting diodes, Appl. Phys. Lett. 97 (2010) 033501.
[33] J. Hader, J.V. Moloney, S.W. Koch, Suppression of carrier recombination in semiconductor lasers by phase-space filling, Appl. Phys. Lett. 87 (2005) 201112.
[34] E. Kioupakis, Q. Yan, D. Steiauf, Van de Walle, G. Chris, Temperature and carrier-density dependence of Auger and radiative recombination in nitride optoelectronic devices, New J. Phys. 15 (2013) 125006.
[35] W. Liu, et al., Carrier-density-dependent recombination dynamics of excitons and electron-hole plasma in m-plane InGaN/GaN quantum wells, Phys. Rev. B 94 (2016) 195411.
[36] D.A. Zakheim, et al., Efficiency droop suppression in InGaN-basedblue LEDs: experiment and numerical modelling, Phys. Status Solidi A 209 (2012) 456–460.
[37] Q. Dai, et al., Carrier recombination mechanisms and efficiency droop in GaInN/GaN light-emitting diodes, Appl. Phys. Lett. 97 (2010) 133507.